

Pulsational instability of supergiant protostars: Do they grow supermassive by accretion?

Kohei Inayoshi¹ ^{*}, Takashi Hosokawa^{2,3} [†], and Kazuyuki Omukai¹ [‡]

¹*Department of Physics, Graduate School of Science, Kyoto University, Kyoto 606-8502, Japan*

²*Department of Physics, University of Tokyo, Tokyo 113-0033, Japan*

³*Jet Propulsion Laboratory, California Institute of Technology, Pasadena CA 91109, USA*

1 September 2018

ABSTRACT

Supermassive stars (SMSs; $M_* \gtrsim 10^5 M_\odot$) and their remnant black holes are promising progenitors for supermassive black holes (SMBHs) observed in the early universe at $z \gtrsim 7$. It has been postulated that SMSs form through very rapid mass accretion onto a protostar at a high rate exceeding $0.01 M_\odot \text{ yr}^{-1}$. According to recent studies, such rapidly accreting protostars evolve into “supergiant protostars”, i.e. protostars consisting of a bloated envelope and a contracting core, similar to giant star. However, like massive stars as well as giant stars, both of which are known to be pulsationally unstable, supergiant protostars may also be also unstable to launch strong pulsation-driven outflows. If this is the case, the stellar growth via accretion will be hindered by the mass loss. We here study the pulsational stability of the supergiant protostars in the mass range $M_* \lesssim 10^3 M_\odot$ through the method of the linear perturbation analysis. We find that the supergiant protostars with $M_* \gtrsim 600 M_\odot$ and very high accretion rate $\dot{M}_{\text{acc}} \gtrsim 1.0 M_\odot \text{ yr}^{-1}$ are unstable due to the κ mechanism. The pulsation is excited in the He^+ ionization layer in the envelope. Even under a conservative assumption that all the pulsation energy is converted into the kinetic energy of the outflows, the mass-loss rate is $\sim 10^{-3} M_\odot \text{ yr}^{-1}$, which is lower than the accretion rate by more than two orders of magnitude. We thus conclude that the supergiant protostars should grow stably via rapid accretion at least in the mass range we studied. As long as the rapid accretion is maintained in the later stage, protostars will become SMSs, which eventually produce seeds for the high- z SMBHs.

Key words: stars: Population III, protostars, oscillations, mass-loss – cosmology: theory – early Universe – galaxies: formation, nuclei

1 INTRODUCTION

Recent observations of high- z quasars reveal that supermassive black holes (SMBHs) of $M_{\text{BH}} \gtrsim 10^9 M_\odot$ have already formed as early as the beginning of the universe $\lesssim 0.8 \text{ Gyr}$ (e.g., Fan 2006; Willott et al. 2007). A popular formation scenario of those SMBHs postulates that remnant stellar-mass BHs ($M_{\text{seed}} \sim 100 M_\odot$) of Population III (Pop III) stars grow in mass via continuous mass accretion and merge (e.g., Haiman & Loeb 2001; Volonteri, Haardt & Madau 2003; Li et al. 2007). Given that the seed BHs grow at the Eddington mass-accretion rate $\dot{M}_{\text{Edd}} = L_{\text{Edd}}/\epsilon c^2$, where L_{Edd} is the Eddington luminosity, and $\epsilon \simeq 0.1$ is the radiative efficiency, the growth time to $10^9 M_\odot$ BHs

is $\sim 0.05 \ln(M_{\text{BH}}/M_{\text{seed}}) \text{ Gyr} \simeq 0.8 \text{ Gyr}$. Since this growth time is as long as the age of the universe at $z \simeq 7$, where the most distant SMBH is observed (Mortlock et al. 2011), the stellar-mass seed is required to keep growing at least with the Eddington rate. However, recent studies show that this is unlikely as the accretion onto the BH, as well as onto the surrounding disk, is easily quenched by strong radiative feedback from the growing BH itself (Johnson & Bromm 2007; Milosavljević, Couch & Bromm 2009; Alvarez, Wise & Abel 2009; Park & Ricotti 2011; Park & Ricotti 2012; Tanaka, Perna & Haiman 2012).

In an alternative scenario, formation of supermassive stars (SMSs; $M_* \gtrsim 10^5 M_\odot$) and their subsequent collapse directly to the BHs in the first galaxies ($z \gtrsim 10$, $T_{\text{vir}} \gtrsim 10^4 \text{ K}$) has been envisaged (e.g., Bromm & Loeb 2003; Begelman, Volonteri & Rees 2006; Lodato & Nataraajan 2006). Here, primordial-gas clouds more massive than $10^5 M_\odot$ are supposed to contract monolithically to form

^{*} E-mail: inayoshi@tap.sphys.kyoto-u.ac.jp

[†] E-mail: takashi.hosokawa@phys.s.u-tokyo.ac.jp

[‡] E-mail: omukai@tap.sphys.kyoto-u.ac.jp

stars without strong fragmentation. Since rapid H₂ cooling causes fragmentation of the primordial gas cloud, for the SMS formation, suppression of H₂ formation is required by some means. Examples of such means are: the photodissociation by far ultraviolet (FUV) radiation from nearby stars (e.g., Omukai 2001; Bromm & Loeb 2003; Omukai, Schneider & Haiman 2008; Regan & Haehnelt 2009a,b; Shang, Bryan, & Haiman 2010; Inayoshi & Omukai 2011; Agarwal et al. 2012; Johnson, Dalla Vecchia & Khochfar 2012), and the collisional dissociation in dense and hot gas (Inayoshi & Omukai 2012). The latter situation can be realized, for example, by the cold-accretion-flow shocks in the first galaxy formation. In both cases, the primordial gas collapses isothermally at $T \simeq 8000$ K via H atomic cooling (Ly α , two-photon, and H⁻ free-bound emission; Omukai 2001) and no major fragmentation is observed in numerical simulations during this phase (Bromm & Loeb 2003; Regan & Haehnelt 2009a, b).

This monolithic contraction of the cloud leads to a formation of a small protostar ($\sim 0.01 M_{\odot}$) at its center. The embryo protostar subsequently grows to a SMS via rapid accretion of the surrounding envelope. This process sounds similar to the case of ordinary Pop III star formation, where H₂ is the efficient coolant. However, there is an important difference; in the H atomic cooling case, the accretion rate onto the protostar is $\sim 0.1 M_{\odot} \text{ yr}^{-1}$, which is much higher than that in the ordinary Pop III case ($\sim 10^{-3} M_{\odot} \text{ yr}^{-1}$). This is due to the high temperature in the atomic cooling cloud ($\simeq 8000$ K) because the accretion rate is set by the temperature in the star-forming cloud as $\dot{M}_{\text{acc}} \sim 10^{-3} M_{\odot} \text{ yr}^{-1} (T/600 \text{ K})^{1.5}$ (Shu 1977; Stahler et al. 1986).

This rapid accretion with $\sim 0.1 M_{\odot} \text{ yr}^{-1}$ drastically changes the protostellar evolution. Figure 1 shows the evolution of the radii of accreting protostars at different accretion rates. In the ordinary Pop III protostar case ($\dot{M}_{\text{acc}} \simeq 10^{-3} M_{\odot} \text{ yr}^{-1}$), after the so-called *adiabatic-accretion phase*, where adiabatic heat input expands the star gradually with mass and the protostar starts to contract by losing its entropy via radiative diffusion (the *Kelvin-Helmholtz contraction*) until the nuclear ignition occurs at the center. The protostar reaches the zero-age main sequence (ZAMS) stage at this point (Stahler, Palla & Salpeter 1986; Omukai & Palla 2001, 2003). On the other hand, with the accretion rate as high as $\dot{M}_{\text{acc}} \gtrsim 0.1 M_{\odot} \text{ yr}^{-1}$, the protostar continues expanding without the KH contraction as recently found by Hosokawa, Omukai & Yorke (2012, hereafter HOY12) (see Figure 1). In such a star, while most of the interior material contracts, the outermost layer significantly swells up like a red-giant star (*“supergiant protostar” phase*). This is because the outer layer absorbs a part of the outward heat flux and obtains a very high specific entropy. Also in this case the contraction at the center ceases with the hydrogen ignition, but the envelope continuously expands with the increase of stellar mass.

If rapid accretion at $\dot{M}_{\text{acc}} \gtrsim 0.1 M_{\odot} \text{ yr}^{-1}$ is maintained, the stellar mass exceeds $10^5 M_{\odot}$ within its lifetime. Such SMSs are general-relativistically unstable (e.g., Zel’dovich & Novikov 1971; Shapiro & Teukolsky 1983) and collapse as a whole to a BH (Shibata & Shapiro 2002), which can be a seed for the SMBHs residing in the early universe ($z \gtrsim 7$). With the stellar mass increasing, however, the stars

become more radiation-pressure dominated and approach a marginally stable state. This may induce pulsational instability of the massive stars and result in mass-loss from the surface. If this mass loss surpasses the accretion onto the star, the stellar growth will be terminated at that point. To see whether the SMS formations are indeed possible in spite of such mass loss, we examine the pulsational stability of the supergiant protostars in this paper.

Pulsational stability of non-accreting Pop III stars has been studied by Baraffe, Heger & Woosley (2001) and Sonoi & Umeda (2012) in the range $120 M_{\odot} \leq M_{*} \leq 3 \times 10^3 M_{\odot}$. They showed that those stars are unstable against pulsation caused by the nuclear burning (the so-called ϵ mechanism), and that the resulting mass-loss rate is $\dot{M}_{\text{loss}} \gtrsim 10^{-5} M_{\odot} \text{ yr}^{-1}$. Gamgami (2007) studied this mass-loss process from the Pop III stars using spherically symmetric hydrodynamical simulations, and showed that pulsation accelerates the surface material to the escape velocity and causes eruptive mass-loss for $M_{*} \gtrsim 500 M_{\odot}$. On the other hand, the Pop I red-giant stars are known to be pulsationally unstable by the opacity-driven mechanism (the so-called κ mechanism, e.g., Li & Gong 1994; Heger et al. 1997), and the typical mass-loss rate is $\sim 10^{-5} M_{\odot} \text{ yr}^{-1}$ (Yoon & Cantiello 2010). With the Pop III composition while having similar structure to the Pop I red-giants, the supergiant protostars can also be pulsationally unstable.

In this paper, we study their stability by performing the linear stability analysis for the mass range $M_{*} \lesssim 10^3 M_{\odot}$, which has been calculated by HOY12. By estimating the mass-loss rate, we discuss whether supergiant protostars grow via accretion despite the pulsation-driven mass loss.

The organization of this paper is as follows. In Section 2, we introduce the method for the linear stability analysis against the pulsation and for the estimation of the mass-loss rates for unstable stars. In Section 3, we present our results and explain how the stability changes with the different stellar masses and accretion rates. Finally, in Section 4, we summarize our study and present our discussions. In Appendix, we describe the details (the basic equations and boundary conditions) of the linear stability analysis.

2 STABILITY ANALYSIS

We study the pulsational stability of protostars growing at constant accretion rates $\dot{M}_{\text{acc}} = 10^{-3}, 0.03, 0.1, 0.3,$ and $1.0 M_{\odot} \text{ yr}^{-1}$, whose structures have been numerically calculated in our previous work (HOY12). Figure 1 presents the evolution of the stellar radii for these rates. We apply the linear stability analysis (see Appendix for the details) to stellar models either in the ZAMS (for $\dot{M}_{\text{acc}} = 10^{-3} M_{\odot} \text{ yr}^{-1}$) or supergiant protostar (for higher accretion rates), indicated by the shaded areas in Figure 1. We consider the perturbations proportional to $e^{i\sigma t}$, where $\sigma = \sigma_{\text{R}} + i\sigma_{\text{I}}$ is the eigen frequency, σ_{R} the frequency of the pulsation, and $|\sigma_{\text{I}}|$ the growing or damping rate of the pulsation depending on its sign; the stars are stable (respectively unstable) if $\sigma_{\text{I}} > 0$ (respectively $\sigma_{\text{I}} < 0$). According to previous studies, massive main-sequence Pop III stars are unstable only under the radial perturbations (Baraffe et al. 2001; Sonoi & Umeda 2012). We thus consider only the radial mode, hereafter, at

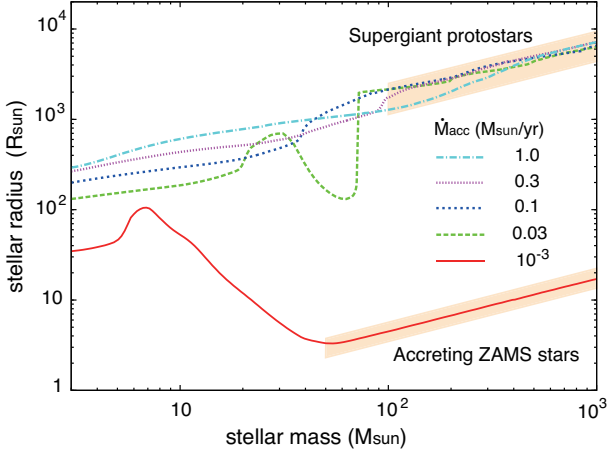


Figure 1. Evolution of the protostellar radius with various accretion rates $\dot{M}_{\text{acc}} = 10^{-3}, 0.03, 0.1, 0.3,$ and $1.0 M_{\odot} \text{ yr}^{-1}$ (taken from HOY12 with some modifications). In this paper, we analyze the pulsational stability of the stars located in the shaded zones; accreting ZAMS stars for $\dot{M}_{\text{acc}} = 10^{-3} M_{\odot} \text{ yr}^{-1}$, and supergiant protostars for $\dot{M}_{\text{acc}} \gtrsim 10^{-3} M_{\odot} \text{ yr}^{-1}$.

which the supergiant protostars are also expected to be the most unstable.

A useful quantity in the stability diagnosis is the work integral W (e.g., Cox 1980; Unno et al. 1989),

$$W(M_r) = \frac{\pi}{\sigma_R} \int_0^{M_r} \Re \left[\frac{\delta T^*}{T} \left(\delta \epsilon - \frac{d}{dM_r} \delta L_{\text{rad}} \right) \right] dM_r, \quad (1)$$

where M_r is the enclosed mass, T is the temperature, ϵ is the nuclear energy generation rate per unit mass, L_{rad} is the radiative luminosity, and the symbols with δ represent the Lagrange perturbations, where symbol \Re denotes the real part of the quantity indicated in the bracket. The work integral has the physical meaning of the pulsation energy gained inside M_r in a single period. If the sign of the work integral is positive at the stellar surface, i.e., $W(M_*) > 0$, the stars gain kinetic energy in each period and are unstable. The pulsation amplitude increases during the growth timescale of the instability σ_1^{-1} . If $W(M_*) < 0$, on the other hand, the pulsation damps inside the stars and are stable. The first term in the bracket on the right-hand side of equation (1), proportional to $\delta \epsilon$, represents the driving of instability by the nuclear burning (i.e., the ϵ mechanism). The second term is related to the radiative energy transport. In most cases, the radiative diffusion damps the pulsation, and thus the second term contributes to the stabilization. However, in the surface layer where the opacity changes remarkably, the energy flux transported via radiation can be absorbed and be converted into the pulsation energy by the κ mechanism. The growth (or damping) rate of the pulsation per single period $\eta \equiv -\sigma_1/\sigma_R$ is written as

$$\eta \equiv -\frac{\sigma_1}{\sigma_R} = \frac{W(M_*)}{4\pi E_W}, \quad (2)$$

(see Cox 1980; Unno et al. 1989), where

$$E_W = \frac{\sigma_R^2}{2} \int_0^{M_*} |\xi_r|^2 dM_r \quad (3)$$

is the pulsation energy, and ξ_r is the radial displacement of fluid elements from their equilibrium positions.

In stars which are unstable under linear perturbations, the pulsation amplitude will grow to the non-linear regime. Such a strong pulsation is expected to cause a mass loss from the stellar surface (Appenzeller 1970a, b; Papaloizou 1973a, b). Appenzeller (1970a, b) studied the non-linear growth of the radial-pulsation instability for Pop I massive stars of $M_* = 130$ and $270 M_{\odot}$ using one-dimensional hydrodynamical calculations. He showed that after the pulsation enters the non-linear regime, the surface velocity reaches the speed of sound and weak shocks emerge just inside the photosphere. The shocks recurrently propagate outward and accelerate the gas in the surface layer (e.g., Lamers & Cassinelli 1999), generating mass shells exceeding the escape velocity which is then lost from the star.

In this paper, we evaluate the mass-loss rate following Baraffe et al. (2001) and Sonoi & Umeda (2012). As shown by Appenzeller (1970a, b), outflows are launched when the pulsation velocity at the surface reaches the speed of sound c_s . At this moment, the pulsation amplitude at the surface is

$$\xi_{r,\text{surf}} = \frac{c_s}{\sigma_R}. \quad (4)$$

Using this, we can estimate the pulsation energy E_W as well as the work integral W . Assuming that all the pulsation energy is converted into the kinetic energy of the outflows, the mass-loss rate \dot{M}_{loss} can be obtained from the energy conservation:

$$\frac{\dot{M}_{\text{loss}}}{2} v_{\text{esc}}^2 = \frac{\sigma_R}{2\pi} W(M_*) = -2\sigma_1 E_W, \quad (5)$$

where $v_{\text{esc}} = (2GM_*/R_*)^{1/2}$ is the escape velocity.

Note that the assumption of energy conservation above is not always valid because some pulsation energy can be lost by radiative dissipation. In fact, Papaloizou (1973a, b) obtains a mass-loss rate lower than that of Appenzeller(1970a, b) by one order of magnitude by including this effect. The mass-loss rate derived below can thus be regarded as a conservative upper limit.

3 RESULTS

In this Section, we describe the results for two different regimes of the accretion rate separately: (a) high accretion-rate cases ($\dot{M}_{\text{acc}} \geq 0.03 M_{\odot} \text{ yr}^{-1}$), where the accreting stars become supergiant protostars, and (b) a low accretion-rate case ($\dot{M}_{\text{acc}} = 10^{-3} M_{\odot} \text{ yr}^{-1}$), where it reaches the ordinary ZAMS. The high-rate regime corresponds to the cases of the SMS formations, while the lower rates are expected in the ordinary Pop III star formation. The latter results are presented for comparison with the previous studies (Baraffe et al. 2001; Sonoi & Umeda 2012). Since we have found that accreting protostars are unstable only for the radial mode without nodes (fundamental mode or ‘‘F-mode’’), we present the results for the F-mode below.

3.1 High accretion-rate cases

($\dot{M}_{\text{acc}} \geq 0.03 M_{\odot} \text{ yr}^{-1}$): supergiant protostars

We see here the high accretion-rate cases $\dot{M}_{\text{acc}} \geq 0.03 M_{\odot} \text{ yr}^{-1}$, where the protostars grow in mass through the supergiant-protostar phase (Figure 1). We first explain

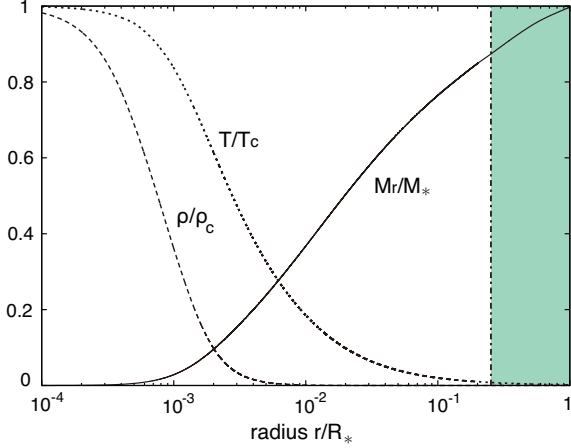


Figure 2. The interior structure of the accreting $10^3 M_{\odot}$ protostar with $\dot{M}_{\text{acc}} = 1.0 M_{\odot} \text{ yr}^{-1}$ as a function of the relative radius r/R_* . The lines present the radial profiles of the enclosed mass (solid), density (dashed), and temperature (dotted), respectively. The enclosed mass is normalized by the stellar mass and others are normalized by their central values; $\rho_c = 0.2 \text{ g cm}^{-3}$ and $T_c = 2.1 \times 10^7 \text{ K}$. The vertical line at $r/R_* \simeq 0.25$ denotes the inner boundary of the convective envelope.

the case with the highest accretion rate $\dot{M}_{\text{acc}} = 1.0 M_{\odot} \text{ yr}^{-1}$ and then the cases with the lower rates.

3.1.1 Highest Accretion-Rate Case ($\dot{M}_{\text{acc}} = 1.0 M_{\odot} \text{ yr}^{-1}$)

Figure 2 shows the stellar interior structure when the stellar mass reaches $10^3 M_{\odot}$ with $\dot{M}_{\text{acc}} = 1.0 M_{\odot} \text{ yr}^{-1}$. No convective core develops in the interior since the hydrogen burning has not yet started. The star instead consists of a radiative core and an outer convective layer. Although the convective layer only constitutes 10% of the stellar mass, and the remaining 90% is the radiative core, it covers a large portion of the radius. This structure consisting of the central core and bloated envelope is similar to that of red-giant stars. With $\dot{M}_{\text{acc}} = 1.0 M_{\odot} \text{ yr}^{-1}$, the protostar reaches this structure at $M_* \gtrsim 200 M_{\odot}$. In this evolutionary stage, the stellar luminosity is close to the Eddington value ($L_* \simeq L_{\text{Edd}} \propto M_*$), and the effective temperature remains almost constant at $T_{\text{eff}} \simeq 5000 \text{ K}$ due to the strong temperature-dependence of the H^- bound-free opacity. With these two conditions, the mass-radius relationship of the supergiant protostars is analytically written as

$$R_* \simeq 8.2 \times 10^3 R_{\odot} \left(\frac{M_*}{10^3 M_{\odot}} \right)^{1/2}, \quad (6)$$

which well agrees with the numerical results (HOY12).

Figure 3 shows the spatial distributions of the work integral for the radial F-mode at the stellar masses of 300, 500, and $10^3 M_{\odot}$. The work integral W changes remarkably near the surface ($\lesssim 3 \times 10^5 \text{ K}$), in particular, around $4 \times 10^4 \text{ K}$, due to a opacity bump by the He^+ ionization. At 300 and $500 M_{\odot}$, the work integrals are negative at the surface and the stars are stable. At $M_* = 10^3 M_{\odot}$, on the other hand, the work integral at the stellar surface is positive, i.e., the protostar is pulsationally unstable by the κ mechanism excited in the He^+ ionization layer.

All the work integrals shown in Figure 3 are constant in the outer H^0 and He^0 ionization layers since the radiative energy transport is efficient enough there. The κ mechanism neither excite nor damp the pulsation. This can be seen by comparing the following two timescales, the cooling time in the layer outside a radius r in the unperturbed state (thermal timescale; e.g., Sonoi & Shibahashi 2011)

$$t_{\text{th}} \equiv \frac{\int_r^{R_*} 4\pi c_P T \rho r^2 dr}{L}, \quad (7)$$

and the period of the pulsation

$$t_{\text{dyn}} \equiv \frac{2\pi}{\sigma_R}. \quad (8)$$

The open circles in the Figure 3 indicate the transition points where the two timescales equal each other ($t_{\text{th}} = t_{\text{dyn}}$). Outside this point, t_{th} is shorter than t_{dyn} as the density and the specific heat decrease outward. We call this region where $t_{\text{th}} < t_{\text{dyn}}$ as the *non-adiabatic zone*. The variation of the work integral is almost zero there because the entropy is rapidly dissipated during a pulsation period. Thus, the surface value of the work integral, which determines the pulsational stability of the star, is fixed at the transition point to the non-adiabatic zone, where $t_{\text{th}} = t_{\text{dyn}}$.

As seen in Figure 3, the surface value of the work integral $W(M_*)$ increases with the stellar mass and eventually becomes positive for $\gtrsim 500 M_{\odot}$: the protostar becomes pulsationally unstable. Since the work integral grows in the He^+ ionization layer inside the transition point but remains constant outside. This increase of the surface value $W(M_*)$ with the stellar mass can be understood by the concomitant outward-shift of the transition point, which in turn can be explained by comparing the two timescales;

$$t_{\text{th}} \propto \frac{R_*^3}{L_*}, \quad (9)$$

and

$$t_{\text{dyn}} \propto \sqrt{\frac{R_*^3}{M_*}} \quad (10)$$

near the surface. In deriving the equation (9), we used the fact that the term $c_P T \rho$ in equation (7) changes only slightly for $T < 4 \times 10^5 \text{ K}$ in the range $10^2 M_{\odot} \lesssim M_* \lesssim 10^3 M_{\odot}$. Note that the dynamical timescale (equation 10) has the same dependence as the free-fall timescale of the star. Eliminating R_* and L_* in equations (9) and (10) with equation (6) and $L_* \simeq L_{\text{Edd}}$, we obtain:

$$\frac{t_{\text{dyn}}}{t_{\text{th}}} \propto M_*^{-1/4}, \quad (11)$$

the thermal timescale becomes longer with respect to the dynamical timescale near the surface with increasing stellar mass. In other words, the surface layer becomes more adiabatic: the non-adiabatic zone on the surface layer becomes thinner and the transition point moves outward as seen in Figure 3. As a result, the surface value of the work integral increases and the stars become more unstable as the stellar mass increase.

The growth rate of the pulsation η and the resulting mass-loss rate \dot{M}_{loss} are shown in Figure 4 as a function of the stellar mass. At $M_* \simeq 600 M_{\odot}$, the star becomes pulsationally unstable and the mass loss rate increases with

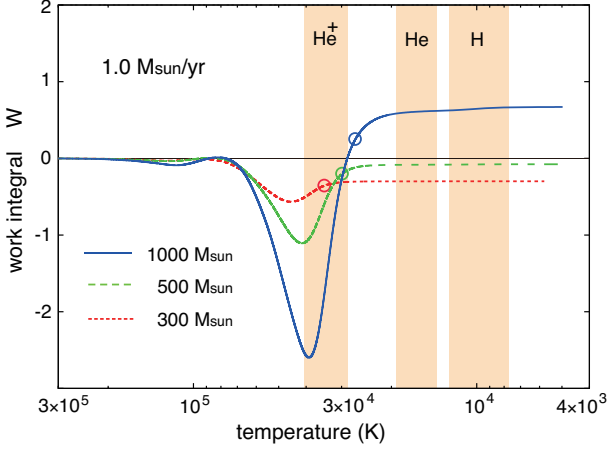


Figure 3. Radial distributions of the work integral W (in an arbitrary unit) near the stellar surface ($T < 3 \times 10^5$ K) for $\dot{M}_{\text{acc}} = 1.0 M_{\odot} \text{ yr}^{-1}$. The lines represent the $M_* = 300$ (dotted), 500 (dashed), and $10^3 M_{\odot}$ (solid) stars. The shaded zones denote the ionization layers of He^+ , He, and H from left to right. Open circles mark the transition points, where the thermal timescale is equal to the dynamical timescale, $t_{\text{th}} = t_{\text{dyn}}$.

the stellar mass thereafter. At $M_* \simeq 10^3 M_{\odot}$, the mass-loss rate reaches $2 \times 10^{-3} M_{\odot} \text{ yr}^{-1}$, two orders of magnitude higher than that in the ZAMS case with accretion rate $\dot{M}_{\text{acc}} = 10^{-3} M_{\odot} \text{ yr}^{-1}$ (see Sec. 3.2 below). This is, however, still lower than the accretion rate by a factor of 500. In the case with spherical symmetry, therefore, pulsation-driven outflow would be completely quenched by the rapid accretion. With some angular momentum, the accretion onto the star proceeds mostly through a circumstellar disk. In this case, the outflow escapes unhindered in the polar directions where the stellar surface is not covered by the accreting flow. We thus expect that the supergiant protostar loses some material via bipolar pulsation-driven outflows, while simultaneously growing in mass due to a more rapid accretion from the disk.

3.1.2 Variation with different accretion rates

Next we see the cases with lower accretion rate $0.03 - 0.3 M_{\odot} \text{ yr}^{-1}$. Figure 5 presents the growth rate η for the radial F-mode in these cases as functions of the stellar mass. Roughly speaking, at a given stellar mass, the growth rate η is higher for higher accretion rates. In our analysis, stars are unstable (i.e. $\eta > 0$) only in the two highest accretion rate cases, those with $1.0 M_{\odot} \text{ yr}^{-1}$ for $M_* \gtrsim 600 M_{\odot}$ and with $0.3 M_{\odot} \text{ yr}^{-1}$ for $M_* \gtrsim 900 M_{\odot}$.

This tendency of instability toward higher accretion rates can be understood again from the outward-shift of the transition point between the adiabatic and non-adiabatic zones inside the He^+ ionization layer, which makes the surface value of the work integral $W(M_*)$ higher (see Section 3.1.1). The behavior of work integral W is shown in Figure 6 for three accretion rates of 0.1, 0.3, and $1.0 M_{\odot} \text{ yr}^{-1}$ at $M_* = 10^3 M_{\odot}$. The ratio of the timescales $t_{\text{dyn}}/t_{\text{th}}$ depends on the accretion rate \dot{M}_{acc} only through the stellar surface luminosity L_* (see equations 6, 7, and 8 and note that the stellar radius is independent of \dot{M}_{acc}). As shown in Figure 7

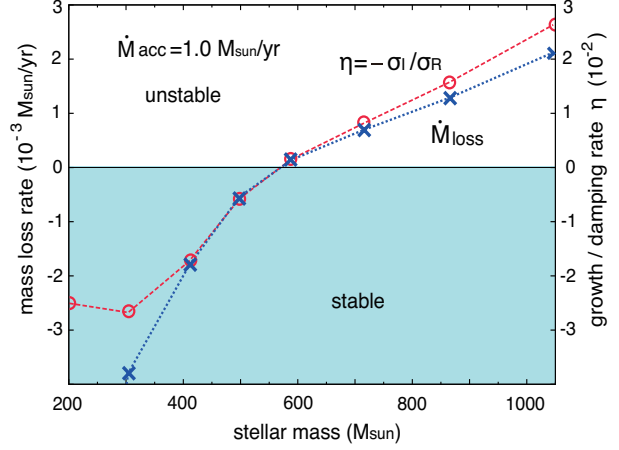


Figure 4. The growth/damping rate $\eta (= -\sigma_I/\sigma_R)$ and the mass-loss rate \dot{M}_{loss} as a function of stellar mass for $\dot{M}_{\text{acc}} = 1.0 M_{\odot} \text{ yr}^{-1}$. The left (right) vertical axis shows \dot{M}_{loss} in unit of $10^{-3} M_{\odot} \text{ yr}^{-1}$ (η in unit of 10^{-2} , respectively). In the shaded area the star is stable against the radial pulsation, i.e., $\eta < 0$.

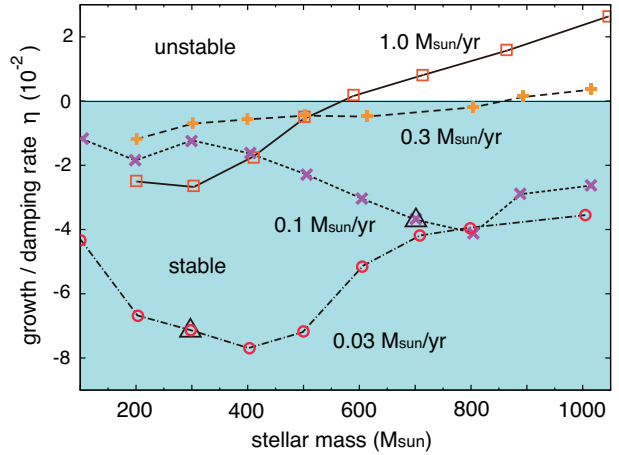


Figure 5. The growth/damping rate $\eta = -\sigma_I/\sigma_R$ as a function of stellar mass for $\dot{M}_{\text{acc}} = 1.0$ (solid), 0.3 (long-dashed), 0.1 (short-dashed), $0.03 M_{\odot} \text{ yr}^{-1}$ (dash-dotted), respectively. In the shaded area the star is stable against the radial pulsation ($\eta < 0$). The symbols on the lines show the models for which we analyze the stability. Large open triangles on the cases with 0.1 and $0.03 M_{\odot} \text{ yr}^{-1}$ indicate the onset of the hydrogen burning.

(a) the surface luminosity L_* and the ratio $t_{\text{dyn}}/t_{\text{th}}$ is lower for higher \dot{M}_{acc} . In other words, the surface region becomes more adiabatic and the transition point moves closer to the surface at higher \dot{M}_{acc} , which makes the surface value of work integral higher as well.

The above relation of L_* and \dot{M}_{acc} can be understood in the following way. With lower \dot{M}_{acc} , the central part of the star has longer time to lose its entropy and the star takes a more centrally concentrated structure at a given stellar mass maintaining the same stellar radius (see Figure 7 b). As the radiative energy transport is efficient in the inner hot and dense part, such a star has larger radiative core. Since the luminosity grows proportionally to the enclosed mass M_r inside the radiative core but remains roughly constant

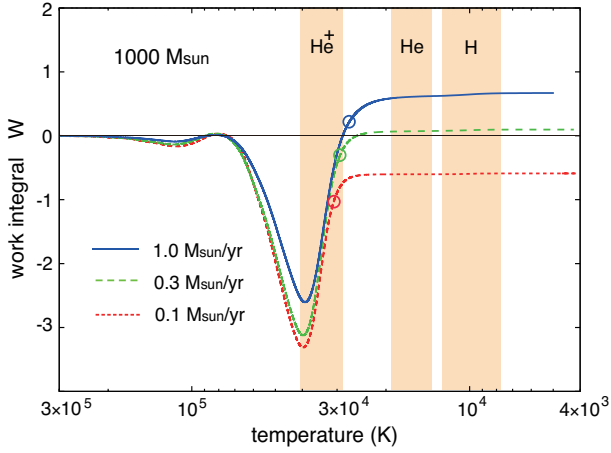


Figure 6. The same as Figure 3, but for the stellar models at $10^3 M_{\odot}$ with three different accretion rates $\dot{M}_{\text{acc}} = 1.0 M_{\odot} \text{ yr}^{-1}$ (solid), $0.3 M_{\odot} \text{ yr}^{-1}$ (dashed), and $0.1 M_{\odot} \text{ yr}^{-1}$ (dotted).

outside (see Figure 7 a), the large radiative core at low \dot{M}_{acc} results in high value of surface luminosity L_* .

Although the overall behavior of the growth rate η shown in Figure 5 can be understood with the above considerations, η evolves in a somewhat complicated way at $\dot{M}_{\text{acc}} = 0.03$ and $0.1 M_{\odot} \text{ yr}^{-1}$; i.e., η decreases with mass early in the evolution. The reason is as follows. As seen above, a supergiant protostar becomes more centrally concentrated and thus more stable (i.e., lower η) with the increasing mass. At the same time, however, there is also a destabilization effect with mass which is due to the shrinking of the non-adiabatic layer of the surface, as discussed in Sec. 3.1.1. These two effects compete each other. With the highest accretion rates of $\dot{M}_{\text{acc}} = 0.3$ and $1.0 M_{\odot} \text{ yr}^{-1}$, the destabilization is more important, while in the cases with low accretion rate of $\dot{M}_{\text{acc}} = 0.03$ and $0.1 M_{\odot} \text{ yr}^{-1}$, the stabilization first dominates until the onset of hydrogen burning, after which the central concentration remains almost constant and the stabilizing effect no longer operates. Thus, at this point η begins to increase as seen in Figure 5.

3.2 Lowest accretion-rate case

($\dot{M}_{\text{acc}} = 10^{-3} M_{\odot} \text{ yr}^{-1}$): **Accreting ZAMS stars**

Next, we will see the lowest accretion-rate case in our calculation with $\dot{M}_{\text{acc}} = 10^{-3} M_{\odot} \text{ yr}^{-1}$, where the protostar reaches the ZAMS at $M_* \simeq 50 M_{\odot}$ after the KH contraction (e.g., Omukai & Palla 2003).

Figure 8 presents the interior structure of the protostar $M_* = 10^3 M_{\odot}$: the radial profiles of the mass, the temperature, the density, and the nuclear energy production rate. The central hydrogen burning via CN-cycle renders the 95% of the stellar mass (covering 60% in radius) to be convective. The vertical line (dot-dashed) in Figure 8 indicates the boundary between the convective core and the outer radiative envelope.

Figure 9 shows the radial distributions of the work integral W , its derivative dW/dM_r , its nuclear-energy production rate ϵ , and its opacity κ within this star. The ϵ -mechanism drives the pulsational instability and thus the

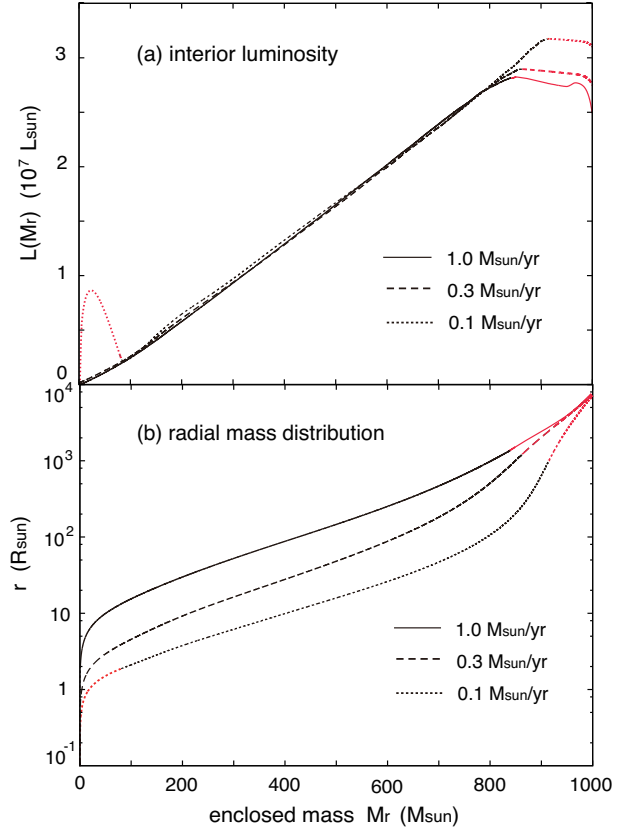


Figure 7. Comparison of the interior structure of $10^3 M_{\odot}$ protostars with different accretion rates. The panels (a) and (b) present the radial distributions of the luminosity and enclosed mass, respectively. In the both panels, the red portions denote the convective zones.

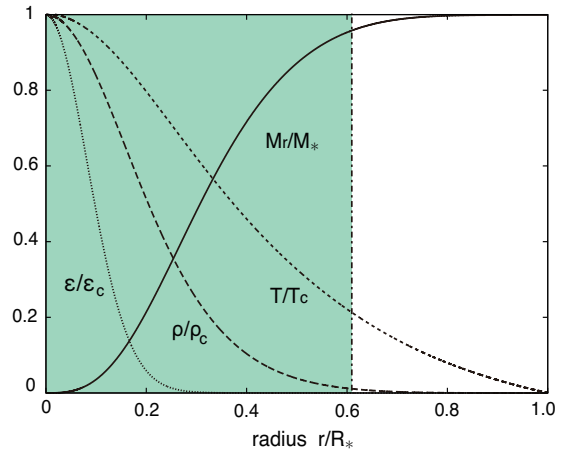


Figure 8. The same as Figure 2, but for the $10^3 M_{\odot}$ protostar with $\dot{M}_{\text{acc}} = 10^{-3} M_{\odot} \text{ yr}^{-1}$. The energy production rate due to the nuclear burning is also shown (dotted). The enclosed mass is normalized by the stellar mass, and others are by their central values: $\rho_c = 11 \text{ g cm}^{-3}$, $T_c = 1.3 \times 10^8 \text{ K}$, and $\epsilon_c = 6.9 \times 10^5 \text{ erg s}^{-1} \text{ g}^{-1}$. The vertical line at $r/R_* \simeq 0.6$ denotes the outer boundary of the convective core.

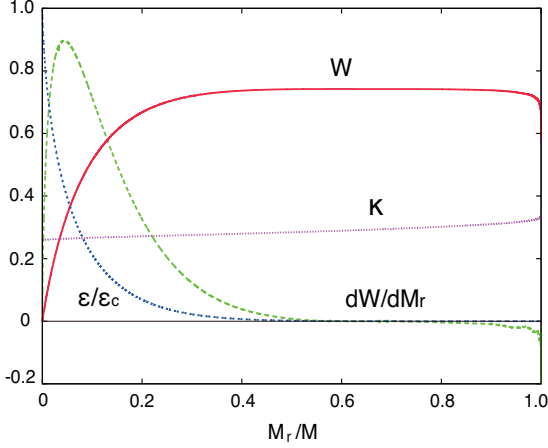


Figure 9. Radial distributions of several quantities within the $M_* = 10^3 M_\odot$ star with $\dot{M}_{\text{acc}} = 10^{-3} M_\odot \text{ yr}^{-1}$. The work integral W (solid line) and its derivative dW/dM_r (long-dashed line) are presented in arbitrary units. The nuclear energy production rate ϵ (normalized by the central value) and the opacity κ (in $\text{cm}^2 \text{ g}^{-1}$) are plotted with the short-dashed and dotted lines, respectively.

work integral W increases inside the convective core. On the other hand, the pulsation is slightly damped (i.e. $dW/dM_r < 0$) in the radiative layer because of the energy dissipation. The κ mechanism does not work as the opacity is almost constant in the envelope due to high surface temperature ($\sim 10^5 \text{ K}$). The small mass inside the surface region cannot totally damp the pulsation excited by the ϵ mechanism. The star is thus unstable, i.e., $W(M_*) > 0$.

Figure 10 presents the growth rate of the pulsation η and the resulting mass-loss rate \dot{M}_{loss} as a function of the stellar mass. After hydrogen ignition at $M_* \simeq 50 M_\odot$, the star remains stable until $140 M_\odot$ when the stabilization by radiative damping overcomes the pulsation by the ϵ mechanism. As the stellar mass increases, however, the star becomes more radiation-pressure dominated and the average adiabatic exponent of the star $\Gamma_1 \equiv (\partial \ln p / \partial \ln \rho)_S$ approaches the marginal gravitational stability value of $4/3$. Consequently, the pulsation becomes increasingly strong in the central convective core and exceeds the radiative damping effect (e.g., Cox 1980; Shapiro & Teukolsky 1983). The star becomes unstable at $140 M_\odot$ and the growth rate of the pulsation increases thereafter. The mass-loss rate is typically $\dot{M}_{\text{loss}} \simeq 10^{-6} - 10^{-5} M_\odot \text{ yr}^{-1}$ (the dotted line in Figure 10). Since this mass-loss rate is lower than the accretion rate $\dot{M}_{\text{acc}} = 10^{-3} M_\odot \text{ yr}^{-1}$, the stellar growth via accretion would not be prevented by the pulsation-driven mass-loss as in the supergiant protostar cases.

Baraffe et al. (2001) and Sonoi & Umeda (2012) also studied the pulsational instability of non-accreting massive Pop III stars. For example, Sonoi & Umeda (2012) estimate the growth rate of the pulsation and mass-loss rate for a $500 M_\odot$ star as $\eta = 3.02 \times 10^{-8}$ and $\dot{M}_{\text{loss}} = 2.0 \times 10^{-5} M_\odot \text{ yr}^{-1}$, respectively. Although their growth rate agrees well with our results, their mass-loss rate is higher than ours by a factor of four. This difference in mass-loss rates comes from the different values of the surface density between the accreting and non-accreting stars. With accre-

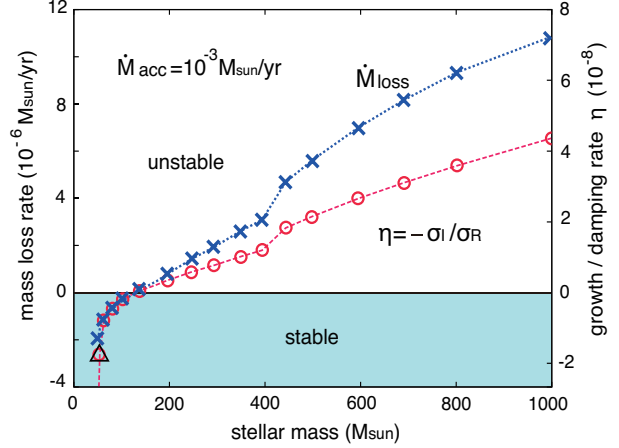


Figure 10. The growth/damping rate $\eta (= -\sigma_I / \sigma_R)$, and the mass loss rate \dot{M}_{loss} as a function of stellar mass for $\dot{M}_{\text{acc}} = 10^{-3} M_\odot \text{ yr}^{-1}$. The left (right) vertical axis shows \dot{M}_{loss} in unit of $10^{-6} M_\odot \text{ yr}^{-1}$ (η in unit of 10^{-8} , respectively). The protostar is stable ($\eta < 0$) against the radial pulsation (F-mode) in the shaded area. Open triangles indicate the onset of the hydrogen burning.

tion, the surface density is higher than that without accretion. In this case, the gas pressure is relatively higher than the radiation pressure, i.e., higher $\beta \equiv p_{\text{gas}} / p_{\text{tot}}$. This results in a lower sound velocity $c_s = \sqrt{\Gamma_1 p / \rho}$ ($\propto \beta^{-1/2}$) at the surface and a lower pulsation amplitude at the onset of the mass loss, which is proportional to the speed of sound (equation 4). Therefore, the pulsation energy E_W and the mass-loss rate become lower in the accreting case than in the non-accreting case.

4 CONCLUSION AND DISCUSSION

In this paper, we have studied the pulsational stability of primordial protostars growing via very rapid accretion, ($\dot{M}_{\text{acc}} \sim 0.1 M_\odot \text{ yr}^{-1}$), through the method of the linear perturbation analysis, which is expected in the case of supermassive star formation in the early universe. We have evaluated mass-loss rate if the protostar is pulsationally unstable and examined whether the mass loss is strong enough to prevent the stellar growth via the accretion. We focused on early stellar evolution of $M_* \lesssim 10^3 M_\odot$, which has been studied in our recent work (HOY12). Our results are summarized as follows.

First, we have studied the high accretion-rate cases with $\dot{M}_{\text{acc}} \gtrsim 0.03 M_\odot \text{ yr}^{-1}$, where the protostar has the a contracting core and a bloated envelope similar to a giant star (*supergiant protostar*; HOY12). With low effective temperature $T_{\text{eff}} \simeq 5000 \text{ K}$, the supergiant protostar has the H and He ionization layers within its envelope. We have found that although pulsation is driven due to blocking of radiative flux at the opacity bump from the He^+ ionization (the so-called κ mechanism), the supergiant protostars are pulsationally unstable only with the highest accretion rate $\simeq 1.0 M_\odot \text{ yr}^{-1}$ we studied. In the lower accretion-rate cases, the protostars are stable at least until $M_* \simeq 10^3 M_\odot$. Even in the most unstable cases, the mass-loss rates are typically

$\sim 10^{-3} M_{\odot} \text{ yr}^{-1}$, which are lower than their accretion rates by more than two orders of magnitude. We thus conclude that the mass loss driven by pulsation does not prevent the growth of the supergiant protostar via rapid accretion.

Next, for comparison with the previous studies, we have analyzed a lower accretion-rate case with $\dot{M}_{\text{acc}} = 10^{-3} M_{\odot} \text{ yr}^{-1}$, which is expected in the ordinary Pop III star formation. In this case, the protostar reaches the ZAMS at $M_* \simeq 50 M_{\odot}$ after the KH contraction stage (e.g., Omukai & Palla 2001, 2003). We have found that the protostars are unstable by the ϵ mechanism in the range $M_* \gtrsim 140 M_{\odot}$, where a large part of the stellar interior is radiation-pressure dominated. Estimated mass-loss rate $10^{-6} - 10^{-5} M_{\odot} \text{ yr}^{-1}$ is roughly consistent with the previous results for non-accreting stars (Baraffe et al. 2001; Sonoi & Umeda 2012) although smaller by few factors because of the difference in the surface density due to the accretion.

In this paper, we have limited our analysis to the mass range $M_* \lesssim 10^3 M_{\odot}$ due to the lack of stellar data in the higher mass range. We here speculate the later evolution based on the current results. Further studies on the protostellar evolution for $M_* > 10^3 M_{\odot}$ as well as on its pulsational stability are thus awaited. If we linearly extrapolate the mass-loss rate in the case of $\dot{M}_{\text{acc}} = 1.0 M_{\odot} \text{ yr}^{-1}$ shown in Figure 4 to higher mass range,

$$\dot{M}_{\text{loss}} \sim 5.0 \times 10^{-4} \left(\frac{M_*}{100 M_{\odot}} - 6 \right) M_{\odot} \text{ yr}^{-1}; \quad (12)$$

the mass loss catches up with the accretion at $M_* \simeq 2 \times 10^5 M_{\odot}$. At this point, the growth of the protostar via accretion possibly halts and the final mass is set. However, because of our assumption that all the pulsation energy is converted to the kinetic energy of the outflows, the mass-loss rate by equation (12) should be regarded as an upper limit (e.g., Papaloizou 1973a, b). Furthermore, the mass loss of the Pop I red-giant stars are usually driven by the radiation pressure exerted on dust grains formed in the cool envelope (e.g., Willson 2000). Without the dust as in our case, acceleration of the outflows could be more inefficient. We expect that, with such rapid accretion, the final stellar mass can exceed $\sim 10^5 M_{\odot}$ despite the pulsation-driven mass loss.

Although mass-loss rate is much lower than the accretion rate until $M_* = 10^3 M_{\odot}$ as studied in this paper, these values could be comparable to $M_* \gtrsim 10^5 M_{\odot}$. Since the accretion of gas with some angular momentum onto the star proceeds via a circumstellar disk, the outflows would escape most easily in the polar regions, where the density is relatively low. The dynamical interaction between the inflows and outflows needs to be studied in detail to determine the exact value of the stellar final mass.

Our estimate of the mass-loss rate is based on the previous works (e.g., Appenzeller 1970a, b; Papaloizou 1973a, b), in which the non-linear development of pulsation for non-accreting main-sequence stars is studied numerically. For the accreting stars, however, we have a very limited knowledge on the non-linear behavior of pulsation (e.g., Gamgami 2007). More detailed studies on this issue by radiative hydrodynamical simulations is awaited.

So far, we have only considered stars forming from the metal-free ($Z = 0$) gas. However, SMSs could potentially be formed from the gas slightly polluted with heavy elements, if that is below the critical amount Z_{cr} , i.e., $\sim 10^{-3} Z_{\odot}$ with-

out dust grains, or $\sim 10^{-5} Z_{\odot}$ with dust grains (Omukai et al. 2008; Inayoshi & Omukai 2012). Metal enrichment lowers the central temperature of a star by enhancing the energy production efficiency by nuclear fusion and also creates another opacity bump near the surface which make the pulsation stronger via the ϵ and κ mechanisms, respectively. However, for the κ mechanism, for which the supergiant protostars are unstable, this effects becomes important only with metallicity higher than $2 \times 10^{-3} Z_{\odot}$ in the case of non-accreting stars (Baraffe et al. 2001), which is higher than the critical value Z_{cr} . We thus speculate that even if small amount of metals below Z_{cr} are present, the pulsational stability of supergiant protostars should be similar to the zero-metallicity case studied above.

Finally, we discuss the validity of the frozen-in approximation of convective energy flux used in our analysis (see Appendix A), where perturbations of the convective flux is neglected. At the present time, this is a widely-used approximation due to our limited knowledge on the interaction between the convective and pulsational motions. Although some other models including this effect have been proposed (e.g., Unno 1967; Gough 1977; Unno et al. 1989; Dupret et al. 2005), they rely on the still-developing time-dependent convection theories, which require different assumptions depending on modeling, beyond the classical mixing-length theory (Böhm-Vitense 1958). Recent results by Penev, Barranco & Sasselov (2009) and Shiode, Quataert & Arras (2012), who studied this interaction numerically, showed that the convective damping weakens the pulsation by the ϵ mechanism, but does not influence through the κ mechanism. Therefore, protostars with modest accretion rate $\dot{M}_{\text{acc}} \simeq 10^{-3} M_{\odot} \text{ yr}^{-1}$, which are unstable by the ϵ mechanism (Sec. 3.2), can be somewhat stabilized by this convective damping. On the other hand, we speculate that this would not significantly affect the pulsation in supergiant protostars, which is driven by the κ mechanism.

ACKNOWLEDGMENTS

We would like to thank Takashi Nakamura for his continuous encouragement, Takafumi Sonoi and Kei Tanaka for fruitful discussions, and Shunsuke Katayama for improving the manuscript. This work is in part supported by the Grants-in-Aid by the Ministry of Education, Culture, and Science of Japan (23-838 KI; 2168407 and 21244021 KO).

APPENDIX A: LINEAR PERTURBATION ANALYSIS METHOD

In this appendix, we describe our method of the linear perturbation analysis of the stellar pulsation stability (e.g., Cox 1980; Unno et al. 1989). The basic equations governing the stellar structure are

$$\frac{\partial \rho}{\partial t} + \nabla \cdot (\rho \mathbf{v}) = 0, \quad (\text{A1})$$

$$\frac{\partial \mathbf{v}}{\partial t} + (\mathbf{v} \cdot \nabla) \mathbf{v} = -\frac{1}{\rho} \nabla p - \nabla \Phi, \quad (\text{A2})$$

$$\nabla^2 \Phi = 4\pi G\rho, \quad (\text{A3})$$

$$T \left[\frac{\partial S}{\partial t} + (\mathbf{v} \cdot \nabla) S \right] = \epsilon - \frac{1}{\rho} \nabla \cdot \mathbf{F}, \quad (\text{A4})$$

$$\mathbf{F}_{\text{rad}} = -\frac{4ac}{3\kappa\rho} T^3 \nabla T, \quad (\text{A5})$$

where ρ is the density, \mathbf{v} the velocity, p the pressure, Φ the gravitational potential, T the temperature, S the specific entropy, ϵ the nuclear-energy generation rate per unit mass, κ the opacity, \mathbf{F} the total energy flux, which is the sum of the radiative flux \mathbf{F}_{rad} and convective flux \mathbf{F}_{conv} , G the gravitational constant, c the speed of light, and a the radiation constant. The radial mode, i.e., perturbations which radially oscillate with an eigen frequency σ , is studied.

We consider the radial displacement of fluid elements from the equilibrium positions in the form $\xi_r(r, t) \equiv \xi_r(r) e^{i\sigma t}$. We define the resulting Euler perturbation of a physical quantity Q as $Q' \equiv Q(r, t) - Q_0(r, t)$, where Q_0 is the value in the unperturbed state. We also use the Lagrange perturbation $\delta Q \equiv Q(r + \xi_r, t) - Q_0(r, t)$ for some physical quantities. The linearized equations (A1)-(A5) with the perturbations $Q'(r, t) = Q'(r) e^{i\sigma t}$ and $\delta Q(r, t) = \delta Q(r) e^{i\sigma t}$ are written as

$$\frac{1}{r^2} \frac{d}{dr} (r^2 \xi_r) - \frac{g}{c_s^2} \xi_r + \frac{p'}{\rho c_s^2} = v_{\text{T}} \frac{\delta S}{c_{\text{P}}}, \quad (\text{A6})$$

$$\frac{1}{\rho} \frac{dp'}{dr} + \frac{g}{\rho c_s^2} p' + (N^2 - \sigma^2) \xi_r + \frac{d\Phi'}{dr} = g v_{\text{T}} \frac{\delta S}{c_{\text{P}}}, \quad (\text{A7})$$

$$\frac{1}{r^2} \frac{d}{dr} \left(r^2 \frac{d\Phi'}{dr} \right) - 4\pi G\rho \left(\frac{p'}{\rho c_s^2} + \frac{N^2}{g} \xi_r \right) = -4\pi G\rho v_{\text{T}} \frac{\delta S}{c_{\text{P}}}, \quad (\text{A8})$$

$$i\sigma T \delta S = \delta\epsilon - \frac{d\delta L_{\text{rad}}}{dM_r}, \quad (\text{A9})$$

$$\frac{\delta L_{\text{rad}}}{L_{\text{rad}}} = -\frac{\delta\kappa}{\kappa} + 4 \frac{\delta T}{T} + 4 \frac{\xi_r}{r} + \frac{d(\frac{\delta T}{T})/d \ln r}{d \ln T/d \ln r}, \quad (\text{A10})$$

where $c_s (= \sqrt{\Gamma_1 p / \rho})$ is the sound velocity, $\Gamma_1 = (\partial \ln p / \partial \ln \rho)_S$ the adiabatic exponent, r the radius, g the gravitational acceleration, L_{rad} the radiative luminosity, M_r the enclosed mass, $c_{\text{P}} = T(\partial S / \partial T)_p$ the isobaric specific heat, $v_{\text{T}} \equiv -(\partial \ln \rho / \partial \ln T)_p$, and $N^2 \equiv -g(d \ln \rho / dr + g/c_s^2)$ the Brunt-Väisärä frequency. In the above equations, for simplicity, a physical quantity “ Q ” indicates its value in the unperturbed state instead of Q_0 .

Note that, in equations (A9) and (A10), we ignore the perturbation of the convective energy flux, i.e., $\delta \mathbf{F}_{\text{conv}} = 0$. This so-called “frozen-in” approximation has been widely used in analyzing the pulsational stability of stars (Baraffe et al. 2001 and Sonoi & Umeda 2012). To facilitate the comparison between their results, we also adopt this assumption here (see Section 4 for more discussions).

From equations (A6) and (A8) and the regularity of Φ' at the center,

$$\frac{d\Phi'}{dr} + 4\pi G\rho \xi_r = 0. \quad (\text{A11})$$

Eliminating the term $d\Phi'/dr$ in equations (A7)-(A10) with

this relation, we obtain four linear ordinary first-order differential equations for four variables ξ_r , p' , δS , and δL_{rad} . Here, we impose the following boundary conditions:

$$\frac{d}{dr} \left(\frac{\xi_r}{r} \right) = 0, \quad \frac{d}{dr} \left(\frac{\delta L_{\text{rad}}}{L_{\text{rad}}} \right) = 0 \quad (r = 0), \quad (\text{A12})$$

$$\frac{d}{dr} \left(\frac{\delta p}{p} \right) = 0 \quad (r = R_*), \quad (\text{A13})$$

from the regularity of the perturbations at the center and surface, and

$$\frac{\delta F_{\text{rad},r}}{F_{\text{rad},r}} = 4 \frac{\delta T}{T} \quad (r = R_*), \quad (\text{A14})$$

which guarantees outward propagation of the energy flux at the surface (e.g., Cox 1980; Saio, Winget & Robinson 1983). In this system of the differential equations and boundary conditions, the normalization of the variables ξ_r , p' , δS , δL_{rad} still remains as a degree of freedom. We solve the system as an eigenvalue problem by formally introducing a differential equation for the eigenvalue σ ,

$$\frac{d\sigma}{dr} = 0. \quad (\text{A15})$$

The whole system here is the five first-order differential equations for ξ_r , p' , δS , δL_{rad} , and σ with the four boundary conditions and one normalization condition. We set the arbitrary normalization condition at the surface, $\xi_r(r = R_*) = R_*$. We obtain numerical solutions of the eigen functions and eigenvalue using the relaxation method (e.g., Unno et al. 1989).

REFERENCES

- Alvarez, M. A., Wise, J. H., & Abel, T. 2009, *ApJL*, 701, L133
- Agarwal, B., Khochfar, S., Johnson, J. L., et al. 2012, *MNRAS*, 425, 2854
- Appenzeller, I. 1970a, *A&A*, 5, 355
- Appenzeller, I. 1970b, *A&A*, 9, 216
- Baraffe, I., Heger, A., & Woosley, S. E. 2001, *ApJ*, 550, 890
- Begelman, M. C., Volonteri, M., & Rees, M. J. 2006, *MNRAS*, 370, 289
- Böhm-Vitense, E. 1958, *Z. Astrophys.*, 46, 108
- Bromm, V., & Loeb, A. 2003, *ApJ*, 596, 34
- Cox, J. P. 1980, *Theory of Stellar Pulsation*, Princeton University Press, Princeton, NJ
- Dupret, M.-A., Grigahcène, A., Garrido, R., Gabriel, M., & Scuflaire, R. 2005, *A&A*, 435, 927
- Fan, X. 2006, *New Astron Rev.*, 50, 665
- Gamgani, F. 2007, Ph.D. Thesis, Heidelberg Univ.
- Gough, D. O. 1977, *ApJ*, 214, 196
- Haiman, Z., & Loeb, A. 2001, *ApJ*, 552, 459
- Heger, A., Jeannin, L., Langer, N., & Baraffe, I. 1997, *A&A*, 327, 224
- Hosokawa, T., Omukai, K., & Yorke, H. W. 2012, *ApJ*, 756, 93 (HOY12)
- Inayoshi, K., & Omukai, K. 2011, *MNRAS*, 416, 2748
- Inayoshi, K., & Omukai, K. 2012, *MNRAS*, 422, 2539
- Johnson, J. L., & Bromm, V. 2007, *MNRAS*, 374, 1557
- Johnson, J. L., Khochfar, S., Greif, T. H., & Durier, F. 2011, *MNRAS*, 410, 919

- Johnson, J. L., Dalla, V. C., & Khochfar, S. 2013, MNRAS, 428, 1857
- Lamers, H. J. G. L. M., & Cassinelli, J. P. 1999, *Introduction to Stellar Winds*, Cambridge University Press, Cambridge, UK
- Li, Y., & Gong, Z. G. 1994, A&A, 289, 449
- Li, Y., et al. 2007, ApJ, 665, 187
- Lodato, G., & Natarajan, P. 2006, MNRAS, 371, 1813
- Milosavljević, M., Couch, S. M., & Bromm, V. 2009, ApJL, 696, L146
- Mortlock, D. J., et al. 2011, Nature, 474, 616
- Omukai, K. 2001, ApJ, 546, 635
- Omukai, K., & Palla, F. 2001, ApJL, 561, L55
- Omukai, K., & Palla, F. 2003, ApJ, 589, 677
- Omukai, K., Schneider, R., & Haiman, Z. 2008, ApJ, 686, 801
- Papaloizou, J. C. B. 1973a, MNRAS, 162, 143
- Papaloizou, J. C. B. 1973b, MNRAS, 162, 169
- Regan, J. A., & Haehnelt, M. G. 2009a, MNRAS, 393, 858
- Regan, J. A., & Haehnelt, M. G. 2009b, MNRAS, 396, 343
- Park, K., & Ricotti, M. 2011, ApJ, 739, 2
- Park, K., & Ricotti, M. 2012, ApJ, 747, 9
- Penev, K., Barranco, J., & Sasselov, D. 2009, ApJ, 705, 285
- Saio, H., Winget, D. E., & Robinson, E. L. 1983, ApJ, 265, 982
- Shang, C., Bryan, G. L., & Haiman, Z. 2010, MNRAS, 402, 1249
- Shapiro, S. L., & Teukolsky, S. A. 1983, *Black Holes, White Dwarfs, and Neutron Stars*. Wiley Interscience, New York
- Shibata, M., & Shapiro, S. L. 2002, ApJL, 572, L39
- Shiode, J. H., Quataert, E., & Arras, P. 2012, MNRAS, 3116
- Shu, F. H. 1977, ApJ, 214, 488
- Sonoi, T., & Umeda, H. 2012, MNRAS, 421, L34
- Sonoi, T., & Shibahashi, H. 2011, PASJ, 63, 95
- Stahler, S. W., Palla, F., & Salpeter, E. E. 1986, ApJ, 302, 590
- Tanaka, T., Perna, R., & Haiman, Z. 2012, MNRAS, 425, 2974
- Unno, W. 1967, PASJ, 19, 140
- Unno, W., Osaki, Y., Ando, H., Saio, H., & Shibahashi, H. 1989, *Nonradial oscillations of stars*, 2nd ed. University of Tokyo Press, Tokyo
- Volonteri, M., Haardt, F., & Madau, P. 2003, ApJ, 582, 559
- Willott, C. J., et al. 2007, AJ, 134, 2435
- Willson, L. A. 2000, ARA&A, 38, 573
- Yoon, S.-C., & Cantiello, M. 2010, ApJL, 717, L62
- Zel'dovich, Y. B., & Novikov, I. D. 1971, *Relativistic Astrophysics, vol. I.: stars and relativity*, Chicago: University of Chicago Press

This paper has been typeset from a \TeX / \LaTeX file prepared by the author.